Cell Reports
Article

Vaccinia Virus Entry Is Followed by Core Activation and Proteasome-Mediated Release of the Immunomodulatory Effector VH1 from Lateral Bodies

Florian Ingo Schmidt,[1,4] Christopher Karl Ernst Bleck,[3,4] Lucia Reh,[1] Karel Novy,[2] Bernd Wollscheid,[2] Ari Helenius,[1] Henning Stahlberg,[3] and Jason Mercer[1,*]
[1]Institute of Biochemistry
[2]Institute of Molecular Systems Biology
ETH Zurich, 8093 Zurich, Switzerland
[3]Center for Cellular Imaging and NanoAnalytics (C-CINA), Biozentrum, University of Basel, 4058 Basel, Switzerland
[4]These authors contributed equally to this work
*Correspondence: jason.mercer@bc.biol.ethz.ch
http://dx.doi.org/10.1016/j.celrep.2013.06.028

SUMMARY

Host cell entry of vaccinia virus, the prototypic poxvirus, involves a membrane fusion event delivering the viral core and two proteinaceous lateral bodies (LBs) into the cytosol. Uncoating of viral cores is poorly characterized, and the composition and function of LBs remains enigmatic. We found that cytosolic cores rapidly dissociated from LBs and expanded in volume, which coincided with reduction of disulfide-bonded core proteins. We identified the abundant phosphoprotein F17, the dual-specificity phosphatase VH1, and the oxidoreductase G4 as bona fide LB components. After reaching the cytosol, F17 was degraded in a proteasome-dependent manner. Proteasome activity, and presumably LB disassembly, was required for the immediate immunomodulatory activity of VH1: dephosphorylation of STAT1 to prevent interferon-γ-mediated antiviral responses. These results reveal a mechanism used by poxviruses to deliver viral enzymes to the host cell cytosol and are likely to facilitate the identification of additional LB-resident viral effectors.

INTRODUCTION

The ultimate goal of a virus particle is to transport a replication-competent viral genome from an infected to a noninfected cell. This involves delivery of the genome and accessory proteins to the cytosol or nucleus. Typically, it also requires uncoating and decondensation of the genome as well as release of any additional factors within the virus particle. Depending on the virus, different strategies are in place to generate favorable conditions for replication of viral genomes, production of viral nonstructural and structural proteins, and assembly of new virus particles. In addition, viruses have evolved a plethora of mechanisms to suppress, modulate, and avoid antiviral defense mechanisms.

Vaccinia virus (VACV), the prototypic poxvirus, is a close relative of variola virus, the causative agent of smallpox (Damon, 2007). During infection, VACV produces two infectious forms, mature virions (MVs) and extracellular virions (EVs), which contain one or two viral membranes, respectively. In both, the viral DNA genome is packaged within a biconcave core flanked on two sides by structures termed lateral bodies (LBs). The LBs are composed of protein (Ichihashi et al., 1984) and have a roughly oblate ellipsoidal shape that fits into the concavities of the viral core (Cyrklaff et al., 2005).

That the protein composition and function of LBs has remained unclear is likely due to the complexity of poxviruses, composed of ~100 structural proteins, and the inability to purify intact LBs from viral particles or infected cells. When the viral envelope is removed using mild detergents, LBs remain associated with cores, suggesting a coherent structure stably anchored to the surface of the core (Easterbrook, 1966). During virus formation, cores and LBs only become visible as distinct structures after a complex morphogenesis process (Condit et al., 2006), which transforms an immature virion filled with amorphous material into an MV with two distinct core layers and LBs. This involves proteolytic cleavage of core proteins and disulfide bond formation within and between viral proteins, a process catalyzed by viral enzymes (Senkevich et al., 2002). The MVs generated are exceptionally resistant to external influences, such as heat and dehydration. They can remain infectious in biological samples for extended times, adding to the potential danger inherent to this large virus family (MacCallum and McDonald, 1957). The elaborate mechanisms of uncoating and activation of the stable "spore-like" particles during cell entry are of particular interest.

MVs and EVs are internalized into host cells by virus-induced macropinocytosis (Huang et al., 2008; Mercer and Helenius, 2008; Schmidt et al., 2011). For both, the final step of entry is the release of the viral core into the host cell cytosol by a membrane fusion event (Moss, 2012). In some VACV strains and

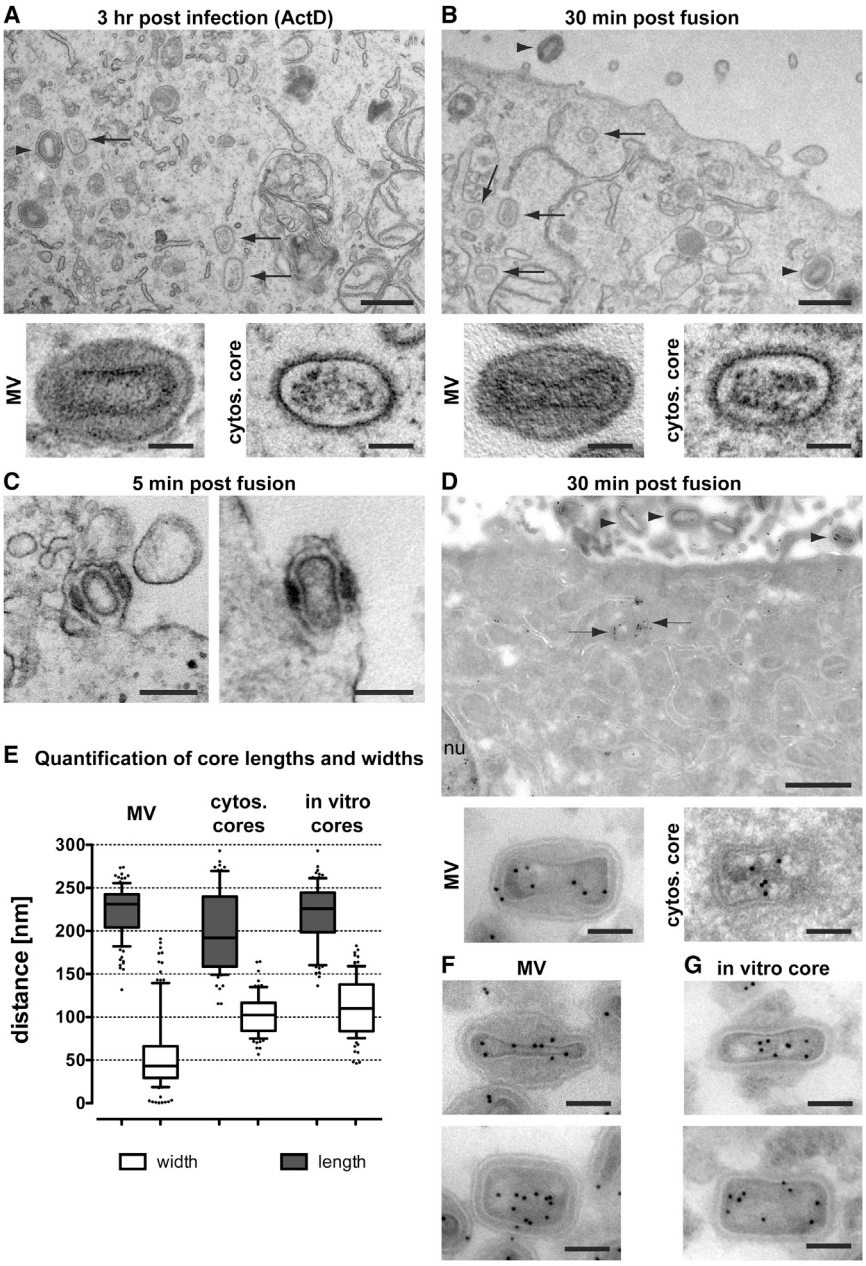

Figure 1. Morphological Changes during VACV Core Activation

(A–D) WR WT MVs were bound to HeLa cells on ice (moi 100) and cells either incubated at 37°C in the presence of ActD (5 μg/ml) for 3 hr (A) or treated with pH 5 medium for 5 min at 37°C followed by either 30 min at 37°C (B and D) or no further incubation (C). Samples were prepared following the protocols for epoxy embedding (A–C) or cryosectioning and anti-DNA immunogold labeling (D). Typical images of thin sections are shown. Bound MVs are highlighted with arrowheads, cytosolic cores with arrows; Nu, nucleus. Scale bars, 500 nm (A, B, and D, top), 100 nm (A, B, and D, bottom), and 200 nm (C).

(E) Quantification of core length and width in MVs, cytosolic cores, and in vitro cores (n = 100). Boxes denote interquartile range, lines within boxes represent the median, whiskers denote 10th and 90th percentiles, and dots show outliers.

(F and G) Representative thin sections of MVs (F) and in vitro cores (G) prepared by cryosectioning and anti-DNA immunogold labeling. Scale bar, 100 nm.

See also Figure S1.

under certain experimental conditions, fusion was also observed at the plasma membrane (Bengali et al., 2012; Chang and Metz, 1976; Chang et al., 2010; Law et al., 2006). The disassembly of viral cores occurs in two steps: in the first, they undergo morphological changes, expand, and take on an oval morphology (Cyrklaff et al., 2007; Dales, 1963; Hollinshead et al., 1999). Transcription of early viral genes is initiated within the core, transcripts are released, and ~80 different early proteins are translated in the cytosol (Yang and Moss, 2009). A second core disassembly step is the genuine uncoating process: the viral DNA genome is released into the cytosol (Joklik, 1964a) and the core is disassembled (Schmidt et al., 2012). This step, needed for replication of the viral DNA, requires the expression of early viral protein(s) and the activity of host factors, including the proteasome (Joklik, 1964b; Mercer et al., 2012). Host cell proteasomes are also required for viral DNA replication (Satheshkumar et al., 2009; Teale et al., 2009).

Although LBs have been visualized by electron microscopy as distinct entities shortly after fusion (Laliberte et al., 2011), their fate and function after virus entry is unknown. That LBs are not visible on cytosolic cores indicates that the association between the two is lost. In this study, we used electron and fluorescence microscopy as well as biochemical techniques to visualize core activation and analyze the composition, function, and fate of LBs of VACV strain Western Reserve (WR). We identified F17, a small phosphoprotein, as the main component of LBs and found that at least one immunomodulatory protein, the viral dual-specificity phosphatase VH1, is brought into cells in LBs and released in a proteasome-dependent manner. A second viral enzyme, the glutaredoxin G4, was also found in LBs.

RESULTS

VACV Cores Undergo Rapid Morphological Changes

Due to the rapid disassembly of incoming cores in the cytosol (Dales, 1963), we used two strategies to enrich this virus structure for visualization in epoxy-embedded electron microscopy (EM) samples: inhibition of early gene expression, a prerequisite for uncoating, using actinomycin D (ActD) (Figure 1A) and low

pH-induced fusion of MVs with the plasma membrane to synchronize core release (Figure 1B; Gong et al., 1990). In both cases, the cores observed in the cytosol were different from cores in intact MVs. Instead of having a biconcave shape, they were larger with an expanded oval or ellipsoidal shape (Figures 1A, 1B, S1A, and S1B). We termed this morphological change core "activation". LBs, which filled the core indentations in MVs, were no longer present.

When analyzed 5 min after acid-induced fusion at the plasma membrane, cores released into the cytosol already exhibited the dilated oval shape (Figure 1C). The LBs remained associated with the fused viral membrane and were no longer attached to the core. The images suggested that the morphological changes in the core occurred during fusion or shortly after exposure of the core to the cytosol and that contact between cores and LBs was concomitantly lost.

To assure that the observed morphological changes were not due to dehydration associated with EM sample processing, EM samples were prepared according to the protocol established by Tokuyasu to better preserve the hydration state of the sample (Slot and Geuze, 2007; Tokuyasu, 1973; Figure 1D). Although LBs could not be readily visualized, the same changes in core morphology were observed under these conditions, indicating that they were not an artifact of sample preparation.

To better understand the requirements of core activation and LB disassociation, we compared cores within MVs to cytosolic cores and cores generated in vitro by removal of the viral membrane with detergent (NP-40) and a reducing agent (dithiothreitol [DTT]) (Easterbrook, 1966; Ichihashi et al., 1984; Figures 1F, 1G, and S1C–S1E). In agreement with the literature (Easterbrook, 1966), in vitro cores were composed of cores and associated LBs. Visualization of LBs depended on core orientation within the section.

We next measured the dimensions of the cores and classified them based on shape as biconcave, oval, or intermediate (Figures 1E and S1F). Cores within MVs had an average central width of 56 nm, and 60% of all cores were classified as biconcave. Cores in the cytosol and those generated in vitro were wider (average central width 103 and 113 nm, respectively) and mostly classified as oval (66% and 57% of all cores, respectively). When core volumes were approximated using the area of the cores in sections (as described in Experimental Procedures; Cyrklaff et al., 2007), cytosolic and in vitro cores exhibited a 1.44- and 1.78-fold larger core volume than those in an MV ($1.263 \cdot 10^6$ nm^3). Thus, the process of cytosolic core activation and in vitro core generation resulted in the loss of core biconcavity, an expansion of its central diameter, and a calculated increase in core volume, perhaps generating space for the transcription process. In contrast to the situation after fusion, LBs remained attached to the core when membranes were removed artificially using NP-40 and DTT. This suggested that membrane removal and reduction of core proteins are sufficient to induce the morphological changes that occur during core activation, whereas LB disassociation requires additional cues.

Viral Core Proteins Are Reduced During Activation

As our in vitro-generated cores resembled activated cytosolic cores and similar morphologies were observed in DTT-treated MVs (Cyrklaff et al., 2007; Locker and Griffiths, 1999), we hypothesized that core activation may involve the reduction of disulfide bonds in viral core proteins. In support of this, two core proteins, 4a and VP8, were shown to be reduced during infection (Locker and Griffiths, 1999). Using redox two-dimensional (2D) SDS-PAGE (Sommer and Traut, 1974) and a combination of sucrose gradients and reducing SDS-PAGE, we identified 13 disulfide-bonded VACV proteins (Figure S2; Table S1). Seven have been described as core-associated: F17 (also known as F18; see Table S2 for nomenclature of VACV proteins), VP8, A4 (also known as A5), 4a, 4b, and the RNA polymerase subunits RPO132 and RPO147. F17, VP8, 4a, and 4b in MVs were disulfide crosslinked into high-molecular-weight complexes. They migrated slowly into or did not enter gels when subjected to nonreducing SDS-PAGE, but migrated as monomers after reduction (Figure 2A). Although the majority of the reduced F17 migrated as expected for monomeric F17, at least three additional slower migrating bands were observed. Anti-hemagglutinin (HA) immunoblots of WR F17-HA MVs confirmed that these were F17 (data not shown). A4 exhibited only intramolecular disulfide bonds and ran faster under nonreducing conditions, due to the more compact structure. High-molecular-weight complexes of RPO132 and RPO147 were confirmed by transient expression of HA-tagged versions in infected cells (data not shown).

To monitor the redox state of the identified proteins during infection, MVs were bound to HeLa cells on ice and harvested or shifted to 37°C for 3 hr in the presence or absence of ActD. Preincubation of MVs with the L1 antibody 7D11 (Wolffe et al., 1995), which blocks core release by MV fusion (Schmidt et al., 2011), served as a control. Cells were harvested and the viral proteins 4b, VP8, and F17 analyzed by nonreducing or reducing SDS-PAGE and immunoblots. Although the majority of these proteins run as monomers upon reduction, no low molecular weight species of F17 or 4b were detected under nonreducing conditions when MVs were prevented from entering host cells (Figure 2B; 0 hr and 3 hr +7D11). At 3 hr post infection, in the absence or presence of ActD, low-molecular-weight bands of F17 and 4b were detected under nonreducing conditions, whereas no changes in the redox state of VP8 were seen. This indicates that F17 and 4b are reduced after deposition of viral cores into the host cytosol, but before early gene transcription (i.e., a stage of infection that coincides with core activation). During these experiments, we observed that the predominant form of F17 was detected at 25 kDa, migrating slightly slower than one of the minor F17 bands found in reduced samples (Figure 2A). When the redox state of F17 was followed during infection using WR F17-HA and HA antibodies, an identical F17 band pattern was seen, ruling out that the bands were nonspecific (Figure 2C).

F17 Is a Major LB Component

With 27,000 copies per MV (Sarov and Joklik, 1972), the phosphoprotein F17 is the third most abundant structural protein of VACV (Chung et al., 2006). Although generally considered a core protein, given that it is present in in vitro-generated cores (Kao and Bauer, 1987; Kao et al., 1981; Sarov and Joklik, 1972), Pedersen et al. (2000) showed that F17 is absent from

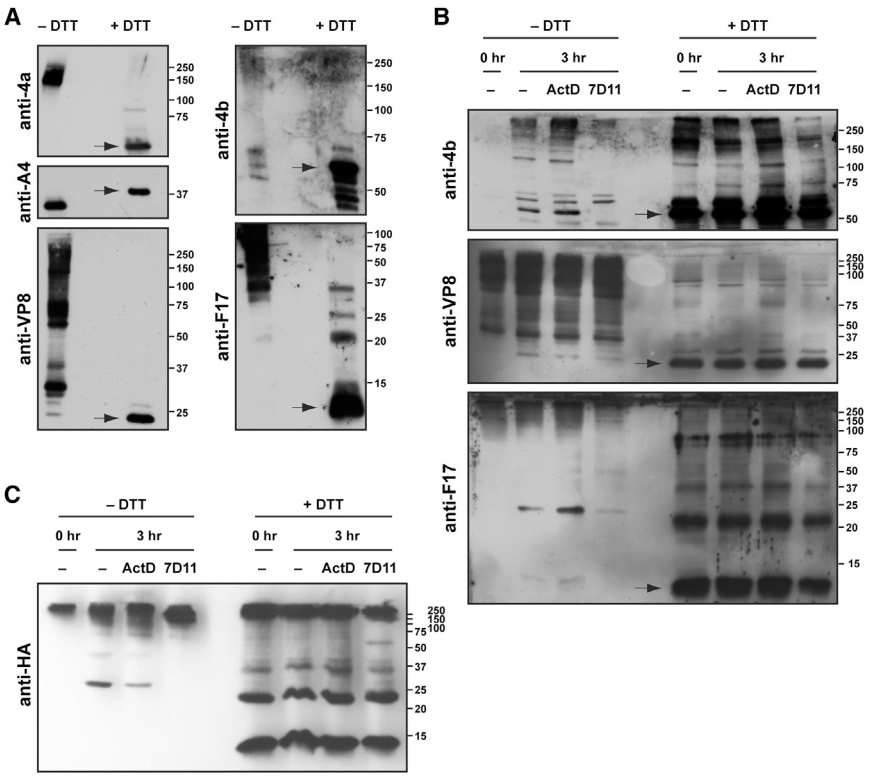

Figure 2. Disulfide-Bonded Viral Proteins Are Reduced during Core Activation

(A) WR WT MVs were alkylated with NEM and boiled in SDS sample buffer without or with DTT. Protein samples were analyzed by SDS-PAGE and immunoblot with the indicated antibodies. Arrows indicate positions of monomeric reduced proteins. The molecular weight marker positions are indicated on the right.

(B and C) WR WT (B) or WR F17-HA (C) MVs were bound to HeLa cells for 1 hr (moi 200) and cells either harvested directly (0 hr) or incubated at 37°C for 3 hr in the absence or presence of ActD. 7D11-neutralized MVs served as controls. Cells were alkylated with NEM and harvested. Protein samples were prepared in SDS sample buffer without or with DTT and analyzed as in (A).

See also Figure S2 and Tables S1 and S2.

cytosolic cores. Using recombinant viruses incorporating either an additional copy of F17 as an EGFP fusion protein or an EGFP fusion of the core protein A4 in combination with anti-GFP immunogold labeling (Figures S3A–S3D), we confirmed these results (Figures 3A–3G). While 94% of cytosolic cores were positive for EGFP-A4, only 14% were positive for EGFP-F17. Thus, EGFP-F17 was largely absent from activated, cytosolic cores.

To determine if F17 was absent from cytosolic cores because it is a LB protein, ultrathin cryosections of MVs and in vitro cores were immunogold labeled with F17 antibodies (Figures 3H, 3I, S3E, and S3F). Quantification showed that, on average, 2.4 and 5.2 gold particles clearly localized to LBs in MVs and in vitro generated cores, respectively (Figure 3K). The few gold particles that localized over the core (0.8 and 1.0 gold particle per core in MVs and in vitro cores, respectively) were likely due to the abundance of F17 and/or the distance between the epitope and the gold particle. Very few gold particles were found outside virion structures.

To verify the localization of F17 to LBs, we treated in vitro cores with a low concentration of trypsin—a method previously used to remove LBs (Easterbrook, 1966; Ichihashi et al., 1984). Trypsin-treated in vitro cores that no longer contained intact LBs were negative for F17 (Figures 3J and S3G). This indicated that F17 labeling depended on intact LBs. While the close proximity of LBs and cores did not allow unambiguous labeling, these results suggested that F17 was present within LBs.

Our initial EM images showed that LBs remained at the virus-derived membrane after acid-induced fusion of MVs (Figure 1C). Five minutes post fusion, we identified viral cores and LBs in close proximity to the plasma membrane (Figures 3L and S3H). More importantly, the distance between cores and LBs was sufficient to unambiguously determine that F17 labeling was exclusively associated with LBs.

To study the fate and localization of F17 and viral cores by fluorescence microscopy, we constructed a virus (WR EGFP-F17 VP8-mCherry) that incorporated EGFP-F17 and an mCherry fusion of a bona fide core protein, the DNA-binding protein VP8 (encoded by the *L4R* gene [Yang et al., 1988]; see Figure S4 for details). Successful incorporation of both proteins into MVs was confirmed by fluorescence microscopy (Figure 4A) and immunoblot analysis (Figures S4C and S4D). Both EGFP-F17 and VP8-mCherry remained associated with in vitro cores, as expected of core and LB components (Figure S4B).

When HeLa cells were infected with WR VP8-mCherry EGFP-F17 for 3 hr in the presence of ActD and analyzed by confocal microscopy, stabilized cytosolic cores did not contain EGFP-F17 (Figure 4C). Conversely, almost all VP8-mCherry-containing cores colocalized with EGFP-F17 in controls where MVs were bound to HeLa cells in the cold to prevent fusion (Figure 4B). Collectively, these results confirmed that F17 was part of the LBs and not present in cytosolic cores after activation.

LB Disassembly Is Aided by Cellular Proteasome Activity

Our EM data suggested that, immediately after fusion, LBs dissociated from cores as distinct structures (Figure 1C), yet we rarely observed intact LBs within host cells by EM at later times. While in the presence of ActD, a few EGFP-F17 punctae corresponding to LBs could be detected; they were far outnumbered by fluorescent cores (Figure 4C). This suggested that free LBs were unstable after delivery to the cytosol and that their disappearance did not depend on early viral gene expression.

To determine if LBs were dispersed or degraded, we used WR F17-HA and tested whether the abundant LB protein F17 was lost from cells in a proteasome-dependent manner. WR

Cell PRESS
Open ACCESS

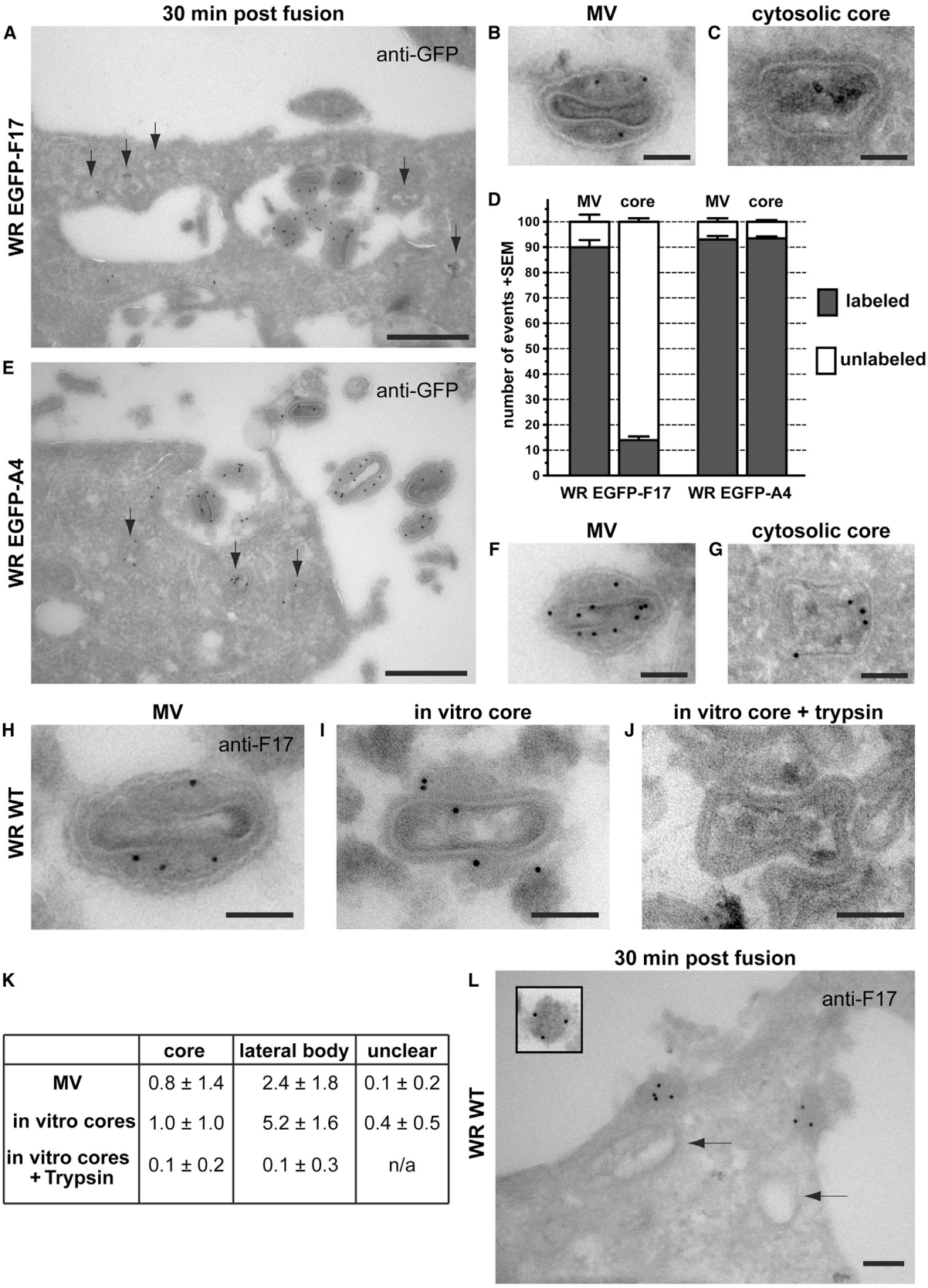

	core	lateral body	unclear
MV	0.8 ± 1.4	2.4 ± 1.8	0.1 ± 0.2
in vitro cores	1.0 ± 1.0	5.2 ± 1.6	0.4 ± 0.5
in vitro cores + Trypsin	0.1 ± 0.2	0.1 ± 0.3	n/a

(legend on next page)

F17-HA MVs were bound to HeLa cells in the cold and the cells harvested directly or after acid-induced fusion and 2 hr at 37°C in the absence or presence of the proteasome inhibitor MG-132 (Rock et al., 1994). ActD was present to prevent viral gene expression. Bound virus particles were removed by trypsin digestion and the cell-associated levels of F17-HA, and the core proteins, VP8 and 4b, were determined (Figure 4E).

In samples harvested 2 hr after fusion, the levels of cell-associated F17 were 3-fold higher in the presence of MG-132, indicating that F17 exposed to the cytosol was degraded by host cell proteasomes. As expected, due to core stabilization by ActD, levels of VP8 and 4b were largely unchanged in the presence or absence of MG-132. In nonsynchronous infection experiments, in which fusion was expected to occur after endocytosis, cell-associated F17 was also stabilized in the presence of proteasome inhibitors 3 hr post infection (Figure S4E). Given that F17 in MVs was detected in immunoblots as multiple bands shifted by ca. 8 kDa, we wondered if the F17 packaged into virions was ubiquitinated. Mass spectrometry-based proteomics was applied to analyze F17-HA immunoprecipitated from MVs solubilized in 1% SDS and 50 mM DTT. We confidently identified 86 peptides of F17-HA, representing a sequence coverage of 97% (Figure S4F) as well as peptides of ubiquitin (data not shown). Several identified peptides of F17 contained lysines with diglycyl adducts—typical remnants of ubiquitination or modification with ubiquitin-like proteins after tryptic digestion. They were confidentially identified on K25, K28, K41, K47, and K50 (Figure S4F). However, no signal was seen when F17-HA was immunoprecipitated and analyzed for conjugated ubiquitin by immunoblot (data not shown). This suggested that ubiquitinated F17 only accounted for a small fraction of the total F17 within MVs and was not the cause of the additional F17 bands observed by immunoblot. The slower migrating F17 bands also occurred when codon-optimized F17-HA was transiently expressed in HeLa cells (data not shown). It is possible that they represent SDS-resistant F17 oligomers.

It was previously reported that F17 was phosphorylated on serines 53 and 62 (Wickramasekera and Traktman, 2010). In MVs, we only detected phosphorylation of F17 S53, S2, and S40, while S62 phosphorylation was never observed, despite the good coverage. Perhaps F17 phosphorylated on S62 is not packaged into MVs or only occurs when S53 is not available. Curiously, although K50 and S53 (as well as K47 in the case of miscleaved peptides) are within the same peptide, phosphorylation and diglycyl adducts on lysines were never observed on the same peptide. This raises the possibility that phosphorylation and ubiquitination of F17 are mutually exclusive.

Consistent with ubiquitination of F17 after entry, we found that a fraction of cell-associated F17-HA ran as a high-molecular-weight smear in MG-132-treated cells 3 hr post infection (Figure S4E). However, due to the small amount of cell-associated F17-HA that could be recovered by immunoprecipitation, we could not determine if this smear was ubiquitinated F17.

To assess if stabilization of F17 by MG-132 correlated with the accumulation of intact LBs, host cells were infected with WR EGFP-F17 VP8-mCherry in the presence of ActD and MG-132. Under these conditions, there was a clear increase in the number of cytoplasmic EGFP-F17 spots devoid of VP8-mCherry (Figure 4D).

These results indicated that LBs dissociate from the core as distinct entities that are subsequently disassembled in host cells by proteasome activity. As F17 was degraded by proteasomes in the same time frame, it is tempting to speculate that degradation of the abundant LB protein F17 triggers LB disintegration. That the number of cores still exceeded the number of F17 spots when proteasomes were inhibited suggested that proteasome activity may not be the sole contributing factor to LB disassembly.

The VACV Dual-Specificity Phosphatase VH1 and Glutaredoxin G4 Are Located in LBs

In infected cells, F17 is phosphorylated by cellular proline-directed kinases and dephosphorylated by the viral dual-specificity phosphatase VH1 (Liu et al., 1995; Wickramasekera and Traktman, 2010). MVs lacking VH1 or those incorporating a F17 mutant that cannot be phosphorylated are impaired in early gene expression (Liu et al., 1995; Wickramasekera and Traktman, 2010). The functional relationship between F17 and VH1 suggested that these proteins may be in close proximity within virions. While VH1 has been shown to be present in cores generated in vitro (Liu et al., 1995), its precise localization within these subviral structures has not been determined.

We generated a virus expressing an HA-tagged version of VH1 and verified by immunoblot that VH1-HA was incorporated into MVs (Figure S5C). Under nonreducing conditions, a fraction of VH1 ran as high-molecular-weight bands, suggesting the protein is partly engaged in intermolecular disulfide bonds. We next analyzed VH1-HA localization by immunogold labeling and EM. MVs of WR VH1-HA were artificially fused to HeLa cells, allowing us to analyze the subviral localization of VH1 in intact MVs at the cell surface and in virus structures shortly after fusion (Figures 5A, 5B, 5E, S5A, and S5B). In bound MVs, an average of 4.1 gold particles was found within the region of LBs, while only

Figure 3. F17 Is Localized to Lateral Bodies

(A–G) MVs of WR EGFP-F17 (A–C) or WR EGFP-A4 (E–G) were bound to HeLa cells on ice (moi 100), treated with pH 5 medium at 37°C for 5 min, and incubated in full medium for 30 min at 37°C. Cells were fixed and subjected to cryosectioning and anti-GFP immunogold labeling. (A) and (E) show typical thin sections; representative MVs and cytosolic cores are displayed in (B)/(F) and (C)/(G), respectively. Arrows indicate cytosolic cores. (D) MVs and cores in thin sections were counted and scored for immunogold labeling of GFP fusion proteins; n = 100 for each. Scale bars, 500 nm (A and E) and 100 nm (B, C, F, and G).

(H–J) Representative micrographs of WR WT MVs (H), in vitro cores (I), and in vitro cores treated with trypsin (J) subjected to cryosectioning and immunogold labeling with anti-F17. Scale bar, 100 nm.

(K) Average number of gold particles in the respective subviral locations ± SD; n = 50 virions; n/a, not applicable.

(L) WR WT MVs were bound to HeLa cells on ice (moi 100), treated with pH 5 medium at 37°C for 5 min, fixed, and subjected to cryosectioning and anti-F17 immunogold labeling. Arrows indicate cytosolic cores; a separate lateral body from (I) is shown in the inset at the same scale.

See also Figure S3.

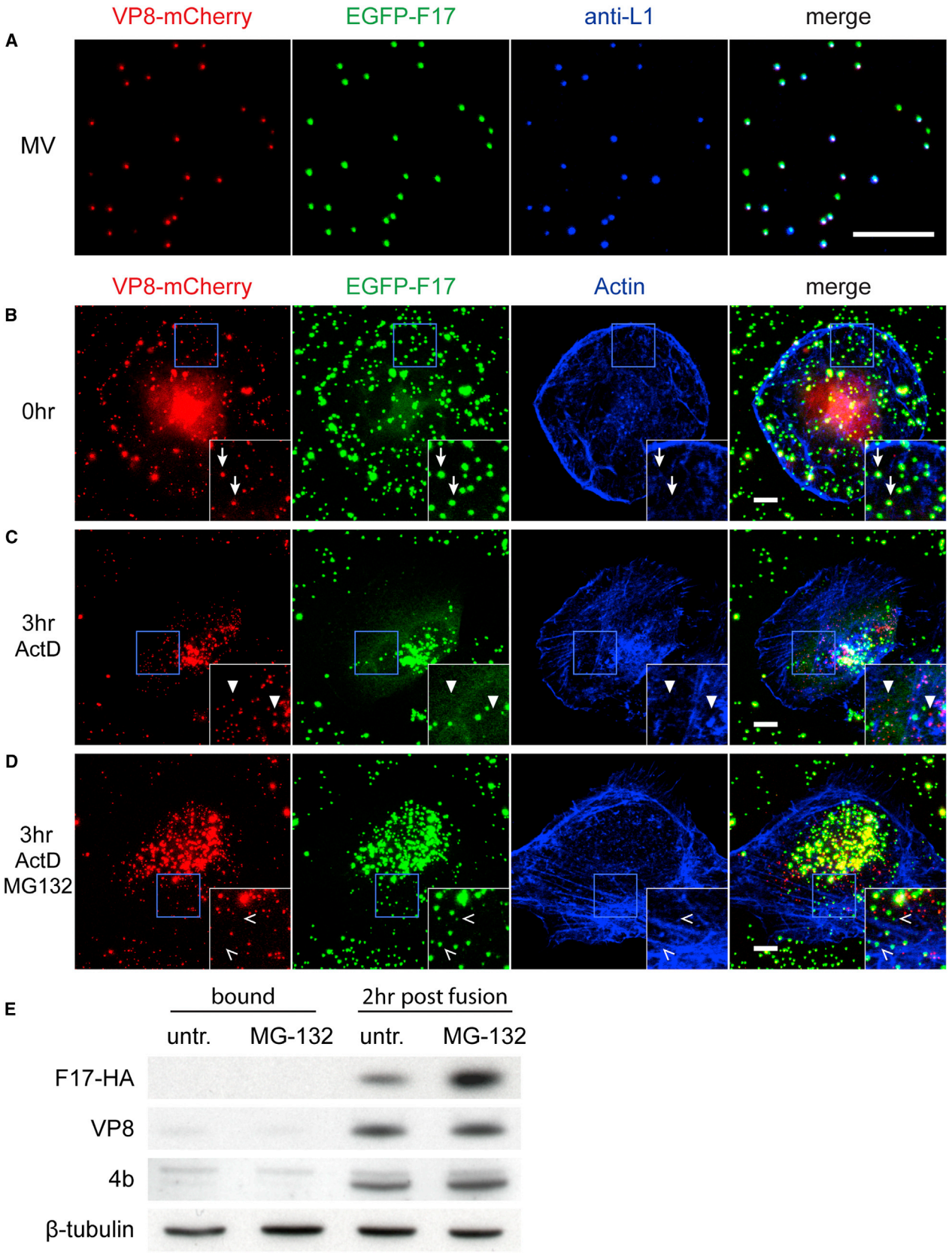

(legend on next page)

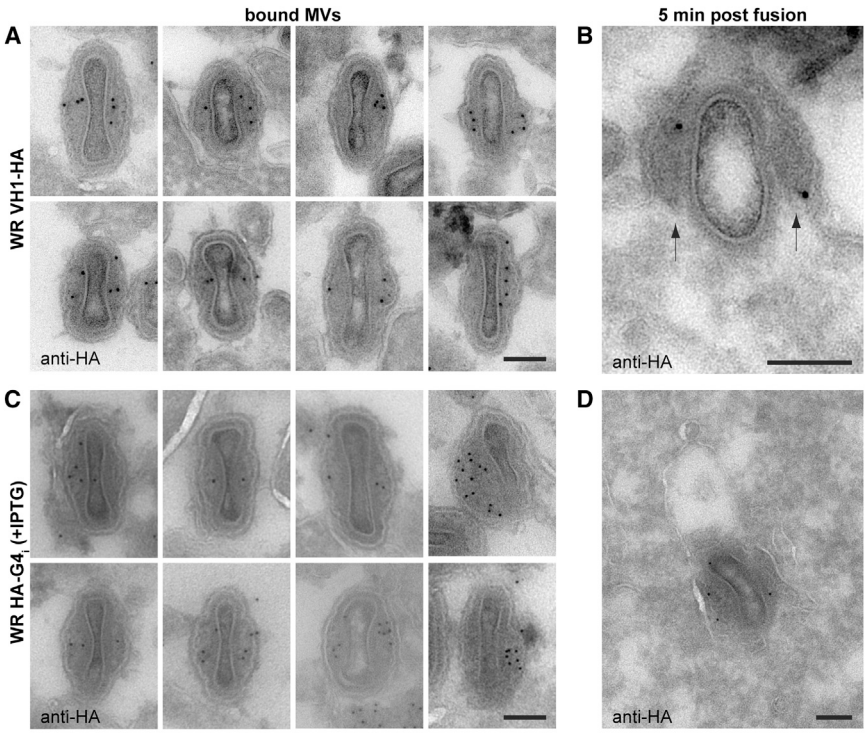

E

	core	lateral body	membrane	unclear
VH1-HA	0.2 ± 0.5	**4.1 ± 1.1**	0.5 ± 0.8	0.3 ± 0.5
HA-G4	0.5 ± 0.9	**2.8 ± 2.7**	0.7 ± 1.0	0.2 ± 0.7
E10-HA	0.3 ± 0.6	0.2 ± 0.4	**1.0 ± 1.0**	0.1 ± 0.2

Figure 5. VH1 and G4 Localize to Lateral Bodies

(A–D) WR VH1-HA MVs (A and B) or WR G4-HA$_i$ MVs produced in the presence of 50 μM isopropyl β-D-1-thiogalactopyranosid (IPTG) (C and D) were bound to HeLa cells on ice (moi 100) and treated with pH 5 medium at 37°C for 5 min. Cells were fixed and subjected to cryosectioning and anti-HA immunogold labeling. Representative bound MVs are displayed in (A) and (C); MVs having just undergone fusion with the plasma membrane are shown in (B) and (D). Arrows indicate LBs; scale bars, 100 nm.

(E) Average number of gold particles in the respective subviral locations ± SD after anti-HA immunogold labeling of bound WR VH1-HA, WR G4-HA$_i$ (+IPTG), and WR E10-HA A2.5-V5 MVs (n = 50, 70, and 69 MVs).

See also Figure S5.

0.2 gold particles were found over the core. In addition, immunogold labeling corresponding to VH1 was found in LBs close to the plasma membrane after acid-induced fusion, with little staining associated with released cores. These results indicated that VH1, like F17, is a component of VACV LBs.

In search of additional LB components, we analyzed three additional viral enzymes known to be incorporated into MVs: the viral kinase B1 as well as G4 and E10, two redox enzymes involved in the formation of cytosolic disulfide bonds during virus assembly (Banham and Smith, 1992; Senkevich et al., 2000; White et al., 2000). Using recombinant viruses that express and subsequently package the HA-tagged variants of the respective proteins (Senkevich et al., 2002; White et al., 2000; data not shown), we performed experiments as described for VH1-HA. These revealed that HA-G4 was predominantly found in LBs (Figures 5C, 5E, and S5D). Consistent with the literature, E10-HA mainly localized to the MV membrane (Figure 5E and S5E), although it acts upstream of G4 in the redox cascade during morphogenesis (Senkevich et al., 2000). The localization of HA-Strep-B1 could not unambiguously be determined, likely due to the low abundance of this kinase in MVs (Chung et al., 2006; Resch et al., 2007; data not shown).

Thus, immunogold labeling of recombinant viruses in combination with electron microscopy allowed us to identify two additional LB components: the viral enzymes VH1 and G4.

The Immunomodulatory Activity of VH1 Depends on Proteasome Activity

The VH1 associated with incoming virus catalyzes the dephosphorylation of the tyrosine-phosphorylated transcription factor STAT1 (p-STAT1) (Najarro et al., 2001). STAT1 is phosphorylated in response to interferon γ (IFNγ) and imported to the nucleus as homodimers, where it mediates the transcription of antiviral and antimicrobial genes (MacMicking, 2012).

Using STAT1 phosphorylation after IFNγ-treatment as a readout for VH1 activity, we asked if LBs have to be disassembled to render VH1 biologically active. HeLa cells infected with wild-type (WT) VACV (or left uninfected) were stimulated

Figure 4. Lateral Bodies Can Be Visualized and Are Stabilized by the Proteasome Inhibitor MG-132

(A) Representative images of WR VP8-mCherry EGFP-F17 MVs bound to coverslips, stained for the MV membrane protein L1, and analyzed by confocal microscopy. Scale bar, 10 μm.

(B–D) WR VP8-mCherry EGFP-F17 MVs were bound to HeLa cells on ice (moi 15). Cells were either fixed directly (B) or incubated at 37°C for 3 hr in the presence of ActD (C) or ActD and 25 μM MG-132 (D). Samples were analyzed by confocal microscopy, and maximal projections of representative Z-stacks are presented. Examples of MVs (arrows), cytosolic cores (closed arrowheads), and free LBs (open arrowheads) are highlighted in the insets. Scale bar, 10 μm.

(E) WR F17-HA MVs were bound to HeLa cells in the cold (moi 10), treated with pH 5 medium at 37°C for 5 min, and harvested directly or incubated in full medium with ActD or ActD and MG-132 for 2 hr at 37°C. During harvest, bound MVs were removed with trypsin. Cells were lysed in SDS sample buffer and proteins analyzed by SDS-PAGE and immunoblot with anti-HA, anti-VP8, anti-4b, and anti-tubulin.

See also Figure S4.

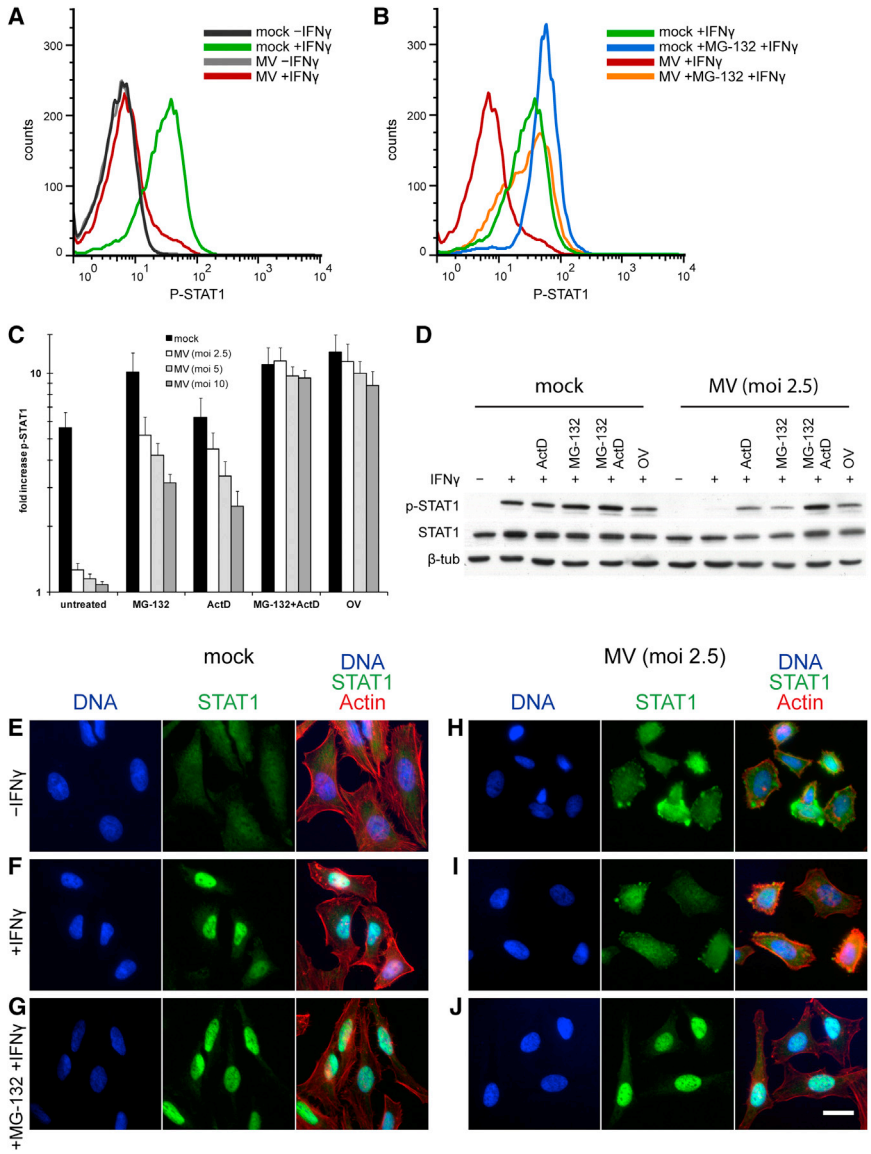

Figure 6. VH1 Activity Requires Proteasome Activity

WR WT MVs (moi 2.5 or as indicated) were bound to HeLa cells in the cold and incubated for 1 hr at 37°C in the presence of the indicated inhibitors (0.75% DMSO (untreated), 5 μg/ml ActD, 25 μM MG-132, or 2 mM orthovanadate [OV]). Cells were subsequently stimulated with IFNγ in the presence of inhibitors for 30 min at 37°C, harvested, and processed for flow cytometry (A–C), immunoblot (D), or fluorescence microscopy (E–J).

(A–C) p-STAT1 levels were quantified by fluorophore-labeled anti-p-STAT1 and flow cytometry. Representative histograms are shown in (A) and (B); average fold increase of p-STAT1 levels upon IFNγ treatment (geometric means) ± SEM from three independent experiments (C).

(D) Cells were lysed and analyzed by SDS-PAGE and immunoblot using the indicated antibodies.

(E–J) Cells were fixed, permeabilized, and stained for STAT1, DNA, and filamentous actin. Samples were analyzed by wide-field fluorescence microscopy. Scale bar, 25 μm.

See also Figure S6.

for 30 min with IFNγ at 1 hr post infection. Samples were then assayed for STAT1 phosphorylation by flow cytometry and immunoblot analysis (Figures 6A–6D). In the absence of infection, IFNγ treatment increased the p-STAT1 signal ~5-fold. Infection with WT VACV at a low multiplicity of infection (moi) prevented STAT1 phosphorylation almost completely (1.2-fold induction) (Figures 6A and 6C). This effect was reverted when VH1 activity was inhibited with orthovanadate, as previously described (Najarro et al., 2001).

To determine if LB disassembly was required for VH1 activity, p-STAT1 levels were assessed in cells infected at an moi of 2.5 in the presence of MG-132. The amount of phosphorylated STAT1 was increased by ~5-fold, indicating that VH1 could not dephosphorylate p-STAT1 in the presence of MG-132 (Figures 6B and 6C). This suggested that proteasome activity was required for full VH1 activity. Inhibition of viral and cellular gene transcription with ActD also partly rescued IFNγ-dependent STAT1 phosphorylation by 4.5-fold (Figure 6C). This was in line with the requirement for cellular gene expression, as previously described (Najarro et al., 2001), or may hint at alternative mechanisms to prevent STAT1 phosphorylation that depend on early viral genes. Early expression of VH1 during infection would explain this phenotype, but the protein was not expressed before DNA replication (Rosel et al., 1986; data not shown). Importantly, orthovanadate, like ActD, completely shut down early viral gene expression, whereas MG-132 reduced it only moderately (Figure S6E). Total STAT1 levels remained constant under all conditions (Figure 6D).

At higher mois, the ability of MG-132 and ActD to prevent the VACV-mediated reduction in STAT1 phosphorylation was overcome. However, when combined, the two inhibitors prevented all viral effects on IFNγ-induced STAT1 phosphorylation, suggesting the drugs target independent processes.

Consistent with its role as an interferon-inducible transcription factor, STAT1 rapidly undergoes nuclear import upon activation. To test if STAT1 phosphorylation correlated with its nuclear translocation and thus biological function, we investigated the subcellular localization of STAT1 during VACV infection using fluorescence microscopy (Figures 6E–6J). In untreated cells, STAT1 was found throughout the cytosol; upon IFNγ stimulation, STAT1 localized predominantly in the nucleus, as expected. When WT VACV-infected cells were treated with IFNγ, STAT1 was found throughout the cytosol, indicating that STAT1 phosphorylation and nuclear import were counteracted by VH1. In

cells infected in the presence of MG-132, nuclear import of STAT1 was restored, consistent with the impairment of VH1-mediated STAT1 dephosphorylation.

Collectively, these results indicated that VH1-mediated dephosphorylation of STAT1 was dependent on proteasome function in host cells. Given that VH1 is active in the absence of any cofactors (Koksal and Cingolani, 2011; Liu et al., 1995), it is probable that the main role of proteasomes is to facilitate LB disassembly. This in turn may result in the liberation of VH1, allowing it to fulfill its effector function prior to early gene expression.

DISCUSSION

After penetration into the cytosol of host cells, incoming viruses and viral capsids have to undergo additional steps before replication can start. With their complex structure and exceptional stability, poxviruses have evolved a stepwise disassembly program dependent on both viral and cellular factors and cues. Our results indicate that the first step in this process, core activation, involves the dissolution of a network of disulfide cross-linked core proteins, which coincides with core expansion and loss of LB core interaction. We identified three poxvirus LB components, among which the dual-specificity phosphatase VH1 exerts an immunomodulatory effector function in the host cell cytosol. We found that both LB disassembly and the phosphatase activity of VH1 require functional proteasomes. We hypothesize that proteasome-mediated release of VH1 from LBs allows VACV to counteract the antiviral response of type II interferons immediately after penetration—at a time when incoming virus particles have yet to undergo gene expression and are likely particularly vulnerable.

Using different EM techniques, we found that, during activation, cores lost their biconcave shape and expanded so that the internal volume increased by ~44%. It is tempting to speculate that reduction of disulfide-bonded 4b and possibly other proteins during activation is required for these morphological changes. Consistent with this, in vitro cores in which all tested disulfide bonds are reduced (data not shown) resemble activated cores. These changes may facilitate the initiation of early transcription. Along these lines, in vitro transcription from cores requires the presence of reducing agents (Munyon et al., 1967). We found that two RNA polymerase subunits were disulfide-bonded; perhaps their reduction activates the RNA polymerase during infection.

Concomitantly with the release of cores into the cytosol, the two proteinaceous LBs of previously unknown composition and function dissociated from the core. Apparently, the interactions that maintain LB association with the core wall, as observed in in vitro cores, were lost. Because the LBs were left behind where the viral and the cellular membranes fused, the interactions with the viral membrane seemed to remain, at least transiently, intact.

In this study, we identified the viral protein F17 as one major LB component. It was previously described as a core or even DNA-binding protein (Ichihashi et al., 1984). Previous studies showed that it interacts with itself and other viral proteins (Mercer and Traktman, 2005; Wickramasekera and Traktman, 2010) and that it localized throughout immature virions and at the core rim in MVs (Traktman et al., 2000). In the absence of F17, VACV exhibits morphogenesis defects: only few aberrant virions were formed that lacked visible LBs (Wickramasekera and Traktman, 2010). These findings are consistent with partitioning of F17 into LBs during morphogenesis.

When followed by fluorescence microscopy, we found that LBs rapidly disappeared as recognizable particles after core release and that this correlated with proteasome-dependent degradation of F17. The observed reduction of disulfide-bonded F17 may contribute to LB disassembly as well, although the LBs of in vitro cores with fully reduced F17 (data not shown) appeared stable. While F17 may have a direct function in host cells, its rapid degradation rather suggests a role as the LB scaffold protein.

We also identified a second LB component, the dual-specificity phosphatase VH1, of which ~200 molecules are packaged per MV (Liu et al., 1995). VH1 is conserved in all poxviruses (Iyer et al., 2006), is essential for the viral life cycle (Liu et al., 1995), and has several viral substrates, including F17, A14, and A17 (Derrien et al., 1999; Liu et al., 1995; Traktman et al., 2000). Immunomodulatory functions of VH1 include the dephosphorylation of the antiviral transcription factor STAT1 and possibly murine STAT2 (Mann et al., 2008; Najarro et al., 2001). In our hands, p-STAT2 levels after IFNα treatment of human cells were not affected by VACV infection (data not shown). VACV replication in several cell lines was sensitive to STAT1-dependent antiviral gene expression induced by IFNγ pretreatment (Terajima and Leporati, 2005; Trilling et al., 2009). Additionally, treatment of VACV-infected mice with IFNγ significantly increased survival (Liu et al., 2004). Collectively, this indicates that VACV needs to interfere with the STAT1-mediated antiviral response for efficient replication.

In our study, p-STAT1 served as a suitable substrate to analyze VH1 activity. We could show that VH1 phosphatase activity on p-STAT1 required functional proteasomes. Given that LBs are stabilized in the presence of proteasome inhibitors and VH1 activity does not require any cofactors (Koksal and Cingolani, 2011), one attractive hypothesis is that incorporation of VH1 in LBs renders the protein inactive and that VH1 has to be released to be catalytically active. The VH1 inhibitor orthovanadate did not lead to the accumulation of LBs (data not shown), suggesting that VH1 activity is not required for LB disassembly.

The viral glutaredoxin G4 was identified as a second catalytically active LB component. Expressed late during infection, G4 is essential for virus morphogenesis (White et al., 2000). It is a component of the VACV-encoded cytoplasmic disulfide-bond formation cascade, consisting of itself, A2.5, and E10. As the last enzyme of this cascade, G4 catalyzes disulfide bond formation in a number of viral membrane proteins, including F9, L1, A21, A28, L5, H2, and A16 (Moss, 2012; Senkevich et al., 2002, 2005). It is likely that E10, A2.5, and G4 also catalyze the formation of disulfide bonds in core and LB proteins. G4 is predominantly packaged in its oxidized form (White et al., 2002). Perhaps G4 oxidizes or reduces its natural substrates during or after entry and may be involved in viral membrane fusion, core activation, or the regulation of LB disassembly.

We concluded that poxvirus LBs serve to transport at least one, and possibly more, effector proteins that act in host cells

prior to viral gene expression. LBs thus comprise a delivery mechanism, presumably conserved across the entire poxvirus family (see Extended Discussion). A similar strategy is used by herpes viruses, such as herpes simplex virus 1, which delivers the virion host shutoff protein and other effectors into cells as part of the tegument, a complex of proteins located inside the particle but outside of the capsid (Smiley, 2004).

Given that the quantified LB components F17 and VH1 only occupy 69% and 1% of the LB mass, respectively (see Extended Experimental Procedures), one can assume the presence of an extra "payload" of additional viral factors. Among these may be viral enzymes that counteract pathogen recognition or modulate the host cell to facilitate virus replication. It is likely that LB-resident proteins also contribute to the cooperativity of VACV early gene expression (Stiefel et al., 2012), where LB proteins could act on viral cores *in trans*. Interestingly, when the first 42 amino acids of F17 were fused to the reporter protein β-galactosidase, the recombinant protein was incorporated into virions and found to be catalytically active in newly infected cells in the absence of viral gene expression (Huang et al., 1988). Perhaps the identification of LB packaging signals will facilitate identification of additional poxvirus effectors.

Deciphering the molecular components and functions of LBs will contribute to a deeper understanding of the early stages of the viral life cycle and probably help further elucidate how poxviruses modulate the host immune system. Moreover, identification of LB packaging signals may allow for artificial targeting of foreign proteins into recombinant poxviruses. Thus, LBs may open attractive possibilities to deliver proteins to cells, to improve poxvirus-based vaccines, and to engineer more potent oncolytic poxviruses.

EXPERIMENTAL PROCEDURES

Cell Lines

BSC-40 (African green monkey) and HeLa (human) cells were cultivated in Dulbecco's modified Eagle's medium (DMEM) (Invitrogen) supplemented with 10% heat-inactivated fetal calf serum (FCS), glutamax, and penicillin-streptomycin; for BSC-40 cells, nonessential amino acids and sodium pyruvate were added in addition.

Viruses

Recombinant vaccinia viruses were generated based on VACV strain WR by transfecting infected cells with plasmids containing genomic viral sequences, as described elsewhere (Mercer and Helenius, 2008; see Extended Experimental Procedures for details on the generation of the respective virions). WR EGFP-A4 was described previously as WR EGFP-A5 (Schmidt et al., 2011); WR HA-G4$_i$ (vG4Li) (White et al., 2000) and WR E10-HA A2.5-V5 (vE10R-HA/A2.5L-V5) (Senkevich et al., 2002) were kind gifts of Bernard Moss (National Institutes of Health). MVs were produced in BSC-40 cells and purified from cytoplasmic lysates, as described elsewhere (Mercer and Helenius, 2008).

Preparation of In Vitro Cores and Other Subviral Particles

In vitro cores were generated by incubating MVs with 1% NP-40 and 50 mM DTT in 10 mM Tris (pH 9.0) for 30 min at 37°C. Cores were sedimented for 1 hr at 16,000 g and 4°C in a tabletop centrifuge and resuspended in 1 mM Tris (pH 9.0). To partially remove LBs, the in vitro core pellet was resuspended in PBS and treated with 20 μg/ml trypsin at 37°C for 15 min. The trypsin digest was stopped with 200 μg/ml aprotinin on ice and virions processed for electron microscopy.

Antibodies and Reagents

A complete list of the used antibodies and reagents is presented in the Extended Experimental Procedures.

Immunoblot

Samples to be analyzed by immunoblot were boiled in SDS sample buffer with 100 mM DTT for 5 min at 95°C. To analyze the redox state of viral proteins, samples were alkylated with 20 mM N-ethylmaleimide (NEM) prior to denaturation and boiled in SDS sample buffer with or without DTT. Proteins were separated on discontinuous SDS-PAGE gels (10% or 15%) or 4%–12% NuPAGE gels (Invitrogen), transferred to nitrocellulose membranes, and analyzed using rabbit anti-4b, anti-4a, anti-A4, anti-VP8, anti-F17, mouse anti-HA (all 1:1,000), rabbit anti-STAT1 (1:500), or rabbit anti-p-STAT1 (1:1,000) in combination with horseradish peroxidase (HRP)-coupled secondary antibodies (1:5,000).

Infection Experiments—Immunofluorescence and Electron Microscopy, Immunoblot

For infection experiments, the indicated amount of MVs were bound to HeLa cells in the cold for 1 hr. Cells were subsequently incubated in full medium at 37°C for the denoted time and processed for immunofluorescence microscopy or different electron microscopy methods. When infection experiments were performed in the presence of drugs, drugs were present during binding and incubation. In some cases, artificial fusion with the plasma membrane was induced after binding by a 5 min treatment with full medium containing 30 mM 2-(N-morpholino)ethanesulfonic acid (MES), pH 5.0, at 37°C. For some immunoblot experiments, bound virions were removed by incubation of cells in 0.25% trypsin (Invitrogen) for 10 min followed by extensive washing in 7% FCS/PBS.

Fluorescence Microscopy

For immunofluorescence microscopy, cells were fixed with 4% formaldehyde (FA) and stained with anti-L1 (0.54 μg/ml) or anti-STAT1 (1 μg/ml) and fluorophore-coupled goat secondary antibodies (1:1,000). Where indicated, actin was stained with fluorophore-coupled phalloidin (1:100) and DNA with Hoechst 33258 (1:10,000). To analyze MVs or in vitro cores, dilutions of the respective samples were bound to coverslips for 20 min, washed, and processed as above. Samples were recorded by confocal microscopy using a Zeiss LSM510 Meta system with a 100X 1.4 numerical aperture (NA) objective.

Sample Processing for Epoxy Embedding EM

Infected cells were fixed and processed for epoxy embedding EM as described elsewhere (Bleck et al., 2010; McDonald, 1984) (see Extended Experimental Procedures for details).

Sample Processing for Immunogold EM According to Tokuyasu

Samples were fixed in 4% FA, 0.1% glutaraldehyde (GA) in 60 mM PIPES, 25 mM HEPES, 10 mM EGTA, and 1 mM $MgCl_2$ (pH 6.9) (PHEM buffer, pH 6.9) (Schliwa et al., 1981). Cells were scraped and sedimented at 500 g; virions or subviral structures were sedimented at 10,500 g. Cryosectioning and immunolabeling were performed as described elsewhere (Slot and Geuze, 2007; Tokuyasu, 1973; see Extended Experimental Procedures for details). In brief, ultrathin sections (50–60 nm) from gelatin-embedded and frozen cell pellets were obtained using an FC7/UC7-ultramicrotome (Leica).

For immunolabeling, cryosections were thawed and incubated with anti-F17 (1:400), anti-GFP (2.5 μg/ml), anti-DNA (0.33 μg/ml), or anti-HA (2 μg/ml). Mouse primary antibodies were detected with polyclonal rabbit anti-mouse immunoglobulin Gs (IgGs) (0.5 μg/ml). All samples were incubated with 5 or 10 nm protein A gold (PAG) (1:60, CMC), as described (Griffiths et al., 1993; Slot and Geuze, 2007), and stained/embedded in 4% uranyl acetate/2% methyl cellulose mixture (ratio 1:9) (Tokuyasu, 1980).

Analysis of Subviral Structures from Electron Micrographs

Thin sections from samples prepared after Tokuyasu (1973) were used for all measurements. To determine the length and width of cores, cores were traced in ImageJ, and processed in Matlab using Dynamo (Castaño-Díez et al., 2012) with an adapted algorithm as follows: The core length was defined as the greatest distance between any two points on a single core outline and

determined the main axis. This axis was divided into three equal segments, and for each, the maximal and minimal widths perpendicular to the main axis were measured. The minimal width in the central segment was used to compare core widths among different cores; box plots were created using GraphPad Prism (GraphPad Software). The core volume was approximated based on the core area (A, determined using ImageJ) as described by Cyrklaff et al. (2007): $V = (\mathrm{sqrt}[A/\pi])^3 4\pi/3$ (n = 100).

Analysis of STAT1 Phosphorylation and Localization

To analyze STAT1 phosphorylation or localization, the indicated amounts of WR WT MVs (+ inhibitors) were bound to pretreated HeLa cells at 4°C for 1 hr and cells were incubated at 37°C for 1 hr (+ inhibitors). Cells were fed with medium containing drugs and 1,000 U/ml IFNγ and harvested 30 min after stimulation at 37°C. For immunoblot analysis, cells were solubilized in SDS sample buffer with phosphatase inhibitors and analyzed as above. To quantify STAT1 phosphorylation by flow cytometry, cells were stained with Alexa Fluor 647 anti-P-STAT1 (1:10) (Schulz et al., 2012). Cells were analyzed using a BD FACSCalibur flow cytometer and the FlowJo software package. For immunofluorescence staining of STAT1, cells were fixed and processed as above and analyzed by wide field fluorescence microscopy using an Olympus Cell˙R imaging station with a 60X 1.4 NA objective.

SUPPLEMENTAL INFORMATION

Supplemental Information includes Extended Discussion, Extended Experimental Procedures, six figures, and two tables and can be found with this article online at http://dx.doi.org/10.1016/j.celrep.2013.06.028.

ACKNOWLEDGMENTS

We thank Paula Traktman for helpful discussions, Daniel Castaño-Diez for help with Dynamo software, Mirko Sobotta for help with redox 2D SDS-PAGE, and Kenneth N. Goldie and Samuel N. Kilcher for critical reading of the manuscript. This work was in part funded by grants from the European Research Council (to A.H.) and the Swiss National Foundation: SystemsX CINA (to C.K.E.B. and H.S.) and InfectX (to A.H.), Ambizione (to J.M.), and Sinergia (to H.S.). F.I.S., A.H., and J.M. conceived the study; F.I.S., C.K.E.B., L.R, and K.N. designed and carried out the experiments; F.I.S., C.K.E.B., and J.M. analyzed the data; B.W. and H.S. gave technical support; and F.I.S., C.K.E.B., A.H., and J.M. wrote the paper.

Received: February 1, 2013
Revised: May 29, 2013
Accepted: June 21, 2013
Published: July 25, 2013

REFERENCES

Banham, A.H., and Smith, G.L. (1992). Vaccinia virus gene B1R encodes a 34-kDa serine/threonine protein kinase that localizes in cytoplasmic factories and is packaged into virions. Virology *191*, 803–812.

Bengali, Z., Satheshkumar, P.S., and Moss, B. (2012). Orthopoxvirus species and strain differences in cell entry. Virology *433*, 506–512.

Bleck, C.K., Merz, A., Gutierrez, M.G., Walther, P., Dubochet, J., Zuber, B., and Griffiths, G. (2010). Comparison of different methods for thin section EM analysis of Mycobacterium smegmatis. J. Microsc. *237*, 23–38.

Castaño-Díez, D., Kudryashev, M., Arheit, M., and Stahlberg, H. (2012). Dynamo: a flexible, user-friendly development tool for subtomogram averaging of cryo-EM data in high-performance computing environments. J. Struct. Biol. *178*, 139–151.

Chang, A., and Metz, D.H. (1976). Further investigations on the mode of entry of vaccinia virus into cells. J. Gen. Virol. *32*, 275–282.

Chang, S.J., Chang, Y.X., Izmailyan, R., Tang, Y.L., and Chang, W. (2010). Vaccinia virus A25 and A26 proteins are fusion suppressors for mature virions and determine strain-specific virus entry pathways into HeLa, CHO-K1, and L cells. J. Virol. *84*, 8422–8432.

Chung, C.S., Chen, C.H., Ho, M.Y., Huang, C.Y., Liao, C.L., and Chang, W. (2006). Vaccinia virus proteome: identification of proteins in vaccinia virus intracellular mature virion particles. J. Virol. *80*, 2127–2140.

Condit, R.C., Moussatche, N., and Traktman, P. (2006). In a nutshell: structure and assembly of the vaccinia virion. Adv. Virus Res. *66*, 31–124.

Cyrklaff, M., Risco, C., Fernández, J.J., Jiménez, M.V., Estéban, M., Baumeister, W., and Carrascosa, J.L. (2005). Cryo-electron tomography of vaccinia virus. Proc. Natl. Acad. Sci. USA *102*, 2772–2777.

Cyrklaff, M., Linaroudis, A., Boicu, M., Chlanda, P., Baumeister, W., Griffiths, G., and Krijnse-Locker, J. (2007). Whole cell cryo-electron tomography reveals distinct disassembly intermediates of vaccinia virus. PLoS ONE *2*, e420.

Dales, S. (1963). The uptake and development of vaccinia virus in strain L cells followed with labeled viral deoxyribonucleic acid. J. Cell Biol. *18*, 51–72.

Damon, I.K. (2007). Poxviruses. In Fields Virology, D.M. Knipe and P.M. Howley, eds. (Philadelphia: Lippincott-Raven), p. 2947.

Derrien, M., Punjabi, A., Khanna, M., Grubisha, O., and Traktman, P. (1999). Tyrosine phosphorylation of A17 during vaccinia virus infection: involvement of the H1 phosphatase and the F10 kinase. J. Virol. *73*, 7287–7296.

Easterbrook, K.B. (1966). Controlled degradation of vaccinia virions in vitro: an electron microscopic study. J. Ultrastruct. Res. *14*, 484–496.

Gong, S.C., Lai, C.F., and Esteban, M. (1990). Vaccinia virus induces cell fusion at acid pH and this activity is mediated by the N-terminus of the 14-kDa virus envelope protein. Virology *178*, 81–91.

Griffiths, G., Burke, B., and Lucocq, J. (1993). Fine structure immunocytochemistry (Berlin: Springer-Verlag).

Hollinshead, M., Vanderplasschen, A., Smith, G.L., and Vaux, D.J. (1999). Vaccinia virus intracellular mature virions contain only one lipid membrane. J. Virol. *73*, 1503–1517.

Huang, C., Samsonoff, W.A., and Grzelecki, A. (1988). Vaccinia virus recombinants expressing an 11-kilodalton beta-galactosidase fusion protein incorporate active beta-galactosidase in virus particles. J. Virol. *62*, 3855–3861.

Huang, C.Y., Lu, T.Y., Bair, C.H., Chang, Y.S., Jwo, J.K., and Chang, W. (2008). A novel cellular protein, VPEF, facilitates vaccinia virus penetration into HeLa cells through fluid phase endocytosis. J. Virol. *82*, 7988–7999.

Ichihashi, Y., Oie, M., and Tsuruhara, T. (1984). Location of DNA-binding proteins and disulfide-linked proteins in vaccinia virus structural elements. J. Virol. *50*, 929–938.

Iyer, L.M., Balaji, S., Koonin, E.V., and Aravind, L. (2006). Evolutionary genomics of nucleo-cytoplasmic large DNA viruses. Virus Res. *117*, 156–184.

Joklik, W.K. (1964a). The Intracellular Uncoating of Poxvirus DNA. I. The Fate of Radioactively-Labeled Rabbitpox Virus. J. Mol. Biol. *8*, 263–276.

Joklik, W.K. (1964b). The intracellular uncoating of poxvirus DNA. II. The molecular basis of the uncoating process. J. Mol. Biol. *8*, 277–288.

Kao, S.Y., and Bauer, W.R. (1987). Biosynthesis and phosphorylation of vaccinia virus structural protein VP11. Virology *159*, 399–407.

Kao, S.Y., Ressner, E., Kates, J., and Bauer, W.R. (1981). Purification and characterization of a superhelix binding protein from vaccinia virus. Virology *111*, 500–508.

Koksal, A.C., and Cingolani, G. (2011). Dimerization of Vaccinia virus VH1 is essential for dephosphorylation of STAT1 at tyrosine 701. J. Biol. Chem. *286*, 14373–14382.

Laliberte, J.P., Weisberg, A.S., and Moss, B. (2011). The membrane fusion step of vaccinia virus entry is cooperatively mediated by multiple viral proteins and host cell components. PLoS Pathog. *7*, e1002446.

Law, M., Carter, G.C., Roberts, K.L., Hollinshead, M., and Smith, G.L. (2006). Ligand-induced and nonfusogenic dissolution of a viral membrane. Proc. Natl. Acad. Sci. USA *103*, 5989–5994.

Liu, K., Lemon, B., and Traktman, P. (1995). The dual-specificity phosphatase encoded by vaccinia virus, VH1, is essential for viral transcription in vivo and in vitro. J. Virol. *69*, 7823–7834.

Liu, G., Zhai, Q., Schaffner, D.J., Wu, A., Yohannes, A., Robinson, T.M., Maland, M., Wells, J., Voss, T.G., Bailey, C., and Alibek, K. (2004). Prevention of lethal respiratory vaccinia infections in mice with interferon-alpha and interferon-gamma. FEMS Immunol. Med. Microbiol. *40*, 201–206.

Locker, J.K., and Griffiths, G. (1999). An unconventional role for cytoplasmic disulfide bonds in vaccinia virus proteins. J. Cell Biol. *144*, 267–279.

MacCallum, F.O., and McDonald, J.R. (1957). Effect of temperatures of up to 45 degrees C on survival of variola virus in human material in relation to laboratory diagnosis. Bull. World Health Organ. *16*, 441–443.

MacMicking, J.D. (2012). Interferon-inducible effector mechanisms in cell-autonomous immunity. Nat. Rev. Immunol. *12*, 367–382.

Mann, B.A., Huang, J.H., Li, P., Chang, H.C., Slee, R.B., O'Sullivan, A., Anita, M., Yeh, N., Klemsz, M.J., Brutkiewicz, R.R., et al. (2008). Vaccinia virus blocks Stat1-dependent and Stat1-independent gene expression induced by type I and type II interferons. J. Interferon Cytokine Res. *28*, 367–380.

McDonald, K. (1984). Osmium ferricyanide fixation improves microfilament preservation and membrane visualization in a variety of animal cell types. J. Ultrastruct. Res. *86*, 107–118.

Mercer, J., and Traktman, P. (2005). Genetic and cell biological characterization of the vaccinia virus A30 and G7 phosphoproteins. J. Virol. *79*, 7146–7161.

Mercer, J., and Helenius, A. (2008). Vaccinia virus uses macropinocytosis and apoptotic mimicry to enter host cells. Science *320*, 531–535.

Mercer, J., Snijder, B., Sacher, R., Burkard, C., Bleck, C.K., Stahlberg, H., Pelkmans, L., and Helenius, A. (2012). RNAi screening reveals proteasome- and Cullin3-dependent stages in vaccinia virus infection. Cell Rep. *2*, 1036–1047.

Moss, B. (2012). Poxvirus cell entry: how many proteins does it take? Viruses *4*, 688–707.

Munyon, W., Paoletti, E., and Grace, J.T., Jr. (1967). RNA polymerase activity in purified infectious vaccinia virus. Proc. Natl. Acad. Sci. USA *58*, 2280–2287.

Najarro, P., Traktman, P., and Lewis, J.A. (2001). Vaccinia virus blocks gamma interferon signal transduction: viral VH1 phosphatase reverses Stat1 activation. J. Virol. *75*, 3185–3196.

Pedersen, K., Snijder, E.J., Schleich, S., Roos, N., Griffiths, G., and Locker, J.K. (2000). Characterization of vaccinia virus intracellular cores: implications for viral uncoating and core structure. J. Virol. *74*, 3525–3536.

Resch, W., Hixson, K.K., Moore, R.J., Lipton, M.S., and Moss, B. (2007). Protein composition of the vaccinia virus mature virion. Virology *358*, 233–247.

Rock, K.L., Gramm, C., Rothstein, L., Clark, K., Stein, R., Dick, L., Hwang, D., and Goldberg, A.L. (1994). Inhibitors of the proteasome block the degradation of most cell proteins and the generation of peptides presented on MHC class I molecules. Cell *78*, 761–771.

Rosel, J.L., Earl, P.L., Weir, J.P., and Moss, B. (1986). Conserved TAAATG sequence at the transcriptional and translational initiation sites of vaccinia virus late genes deduced by structural and functional analysis of the HindIII H genome fragment. J. Virol. *60*, 436–449.

Sarov, I., and Joklik, W.K. (1972). Studies on the nature and location of the capsid polypeptides of vaccinia virions. Virology *50*, 579–592.

Satheshkumar, P.S., Anton, L.C., Sanz, P., and Moss, B. (2009). Inhibition of the ubiquitin-proteasome system prevents vaccinia virus DNA replication and expression of intermediate and late genes. J. Virol. *83*, 2469–2479.

Schliwa, M., Euteneuer, U., Bulinski, J.C., and Izant, J.G. (1981). Calcium lability of cytoplasmic microtubules and its modulation by microtubule-associated proteins. Proc. Natl. Acad. Sci. USA *78*, 1037–1041.

Schmidt, F.I., Bleck, C.K., Helenius, A., and Mercer, J. (2011). Vaccinia extracellular virions enter cells by macropinocytosis and acid-activated membrane rupture. EMBO J. *30*, 3647–3661.

Schmidt, F.I., Bleck, C.K., and Mercer, J. (2012). Poxvirus host cell entry. Curr. Opin. Virol. *2*, 20–27.

Schulz, K.R., Danna, E.A., Krutzik, P.O., and Nolan, G.P. (2012). Single-cell phospho-protein analysis by flow cytometry. Curr. Protoc. Immunol. *Chapter 8*, Unit 8.17.

Senkevich, T.G., Weisberg, A.S., and Moss, B. (2000). Vaccinia virus E10R protein is associated with the membranes of intracellular mature virions and has a role in morphogenesis. Virology *278*, 244–252.

Senkevich, T.G., White, C.L., Koonin, E.V., and Moss, B. (2002). Complete pathway for protein disulfide bond formation encoded by poxviruses. Proc. Natl. Acad. Sci. USA *99*, 6667–6672.

Senkevich, T.G., Ojeda, S., Townsley, A., Nelson, G.E., and Moss, B. (2005). Poxvirus multiprotein entry-fusion complex. Proc. Natl. Acad. Sci. USA *102*, 18572–18577.

Slot, J.W., and Geuze, H.J. (2007). Cryosectioning and immunolabeling. Nat. Protoc. *2*, 2480–2491.

Smiley, J.R. (2004). Herpes simplex virus virion host shutoff protein: immune evasion mediated by a viral RNase? J. Virol. *78*, 1063–1068.

Sommer, A., and Traut, R.R. (1974). Diagonal polyacrylamide-dodecyl sulfate gel electrophoresis for the identification of ribosomal proteins crosslinked with methyl-4-mercaptobutyrimidate. Proc. Natl. Acad. Sci. USA *71*, 3946–3950.

Stiefel, P., Schmidt, F.I., Dörig, P., Behr, P., Zambelli, T., Vorholt, J.A., and Mercer, J. (2012). Cooperative vaccinia infection demonstrated at the single-cell level using FluidFM. Nano Lett. *12*, 4219–4227.

Teale, A., Campbell, S., Van Buuren, N., Magee, W.C., Watmough, K., Coutu-rier, B., Shipclark, R., and Barry, M. (2009). Orthopoxviruses require a functional ubiquitin-proteasome system for productive replication. J. Virol. *83*, 2099–2108.

Terajima, M., and Leporati, A.M. (2005). Role of Indoleamine 2,3-Dioxygenase in Antiviral Activity of Interferon-gamma Against Vaccinia Virus. Viral Immunol. *18*, 722–729.

Tokuyasu, K.T. (1973). A technique for ultracryotomy of cell suspensions and tissues. J. Cell Biol. *57*, 551–565.

Tokuyasu, K.T. (1980). Immunochemistry on ultrathin frozen sections. Histochem. J. *12*, 381–403.

Traktman, P., Liu, K., DeMasi, J., Rollins, R., Jesty, S., and Unger, B. (2000). Elucidating the essential role of the A14 phosphoprotein in vaccinia virus morphogenesis: construction and characterization of a tetracycline-inducible recombinant. J. Virol. *74*, 3682–3695.

Trilling, M., Le, V.T., Zimmermann, A., Ludwig, H., Pfeffer, K., Sutter, G., Smith, G.L., and Hengel, H. (2009). Gamma interferon-induced interferon regulatory factor 1-dependent antiviral response inhibits vaccinia virus replication in mouse but not human fibroblasts. J. Virol. *83*, 3684–3695.

White, C.L., Weisberg, A.S., and Moss, B. (2000). A glutaredoxin, encoded by the G4L gene of vaccinia virus, is essential for virion morphogenesis. J. Virol. *74*, 9175–9183.

White, C.L., Senkevich, T.G., and Moss, B. (2002). Vaccinia virus G4L glutaredoxin is an essential intermediate of a cytoplasmic disulfide bond pathway required for virion assembly. J. Virol. *76*, 467–472.

Wickramasekera, N.T., and Traktman, P. (2010). Structure/Function analysis of the vaccinia virus F18 phosphoprotein, an abundant core component required for virion maturation and infectivity. J. Virol. *84*, 6846–6860.

Wolffe, E.J., Vijaya, S., and Moss, B. (1995). A myristylated membrane protein encoded by the vaccinia virus L1R open reading frame is the target of potent neutralizing monoclonal antibodies. Virology *211*, 53–63.

Yang, Z., and Moss, B. (2009). Interaction of the vaccinia virus RNA polymerase-associated 94-kilodalton protein with the early transcription factor. J. Virol. *83*, 12018–12026.

Yang, W.P., Kao, S.Y., and Bauer, W.R. (1988). Biosynthesis and post-translational cleavage of vaccinia virus structural protein VP8. Virology *167*, 585–590.